Computers & Structures Vol. 39, No. 3/4, pp. 231–242, 1991
Printed in Great Britain.

0045-7949/91 $3.00 + 0.00
Pergamon Press plc

ANALYSIS OF EDGE DELAMINATIONS IN LAMINATES THROUGH COMBINED USE OF QUASI-THREE-DIMENSIONAL, EIGHT-NODED, TWO-NODED AND TRANSITION ELEMENTS

C. G. Shah† and A. V. Krishna Murty‡

†Structural Sciences Division, National Aeronautical Laboratory, Bangalore, India

‡Department of Aerospace Engineering, Indian Institute of Science, Bangalore, India

(*Received* 1 *March* 1990)

Abstract—The use of appropriate finite elements in different regions of a stressed solid can be expected to be economical in computing its stress response. This concept is exploited here in studying stresses near free edges in laminated coupons. The well known free edge problem of $[0/90]_s$ symmetric laminate is considered to illustrate the application of the concept. The laminate is modelled as a combination of three distinct regions. Quasi-three-dimensional eight-noded quadrilateral isoparametric elements (Q3D8) are used at and near the free edge of the laminate and two-noded line elements (Q3D2) are used in the region away from the free edge. A transition element (Q3DT) provides a smooth inter-phase zone between the two regions. Significant reduction in the problem size and hence in the computational time and cost have been achieved at almost no loss of accuracy.

NOTATION

b	halfwidth of the laminate
E_{ii}	modulus of elasticity for orthotropic material in the i-direction, MPa
G	total strain energy release rate
G_I, G_{II}, G_{III}	mode I, mode II and mode III components of strain energy release rate, respectively
l	length (Q3D2 element)
$T = 2H$	laminate thickness, m
G_{ij}	shear modulus for orthotropic material, MPa
h	ply thickness, m
U, V, W	displacement functions (function of y and z in Q3D8 element, function of y only in Q3D2 element), m
u, v, w	displacements in the x-, y- and z-directions, m
x, y, z	Cartesian coordinates, m
ϵ_0	uniform axial strain in the x-direction
η, ζ	nondimensionalized coordinates (see Fig. A1)
Θ	angle between x-axis and longitudinal axis of the ply (see Fig. 1a), degrees
ν_{ij}	Poisson's ratio for orthotropic material
$\{g\}$	vector of Cartesian strains
$\{\sigma\}$	vector of Cartesian stresses

INTRODUCTION

Laminated composites are replacing metals in several engineering applications. The inherent weakness of the resin in a laminate demands new design requirements, such as estimation of interlaminar stresses near cut-outs, free edges, rivet holes, etc., and assessment of the 'delamination tolerance ability' of the structure which, in turn, calls for accurate estimation of the stress field and strain energy release rates.

Laminates are usually treated as a stack of plies bonded together so that no slippage at the interlaminar surface is possible. Each ply is considered as a homogeneous orthotropic medium, with the axes of orthotropy coinciding with the material axes. Modelling of the stress field in such a material system is not an easy task. Theoretical modelling of laminates has been receiving a great deal of attention in recent years. Pioneering works of Pagano and his associates [1, 2], displacment-based models studied by various others [3], iterative modelling possibilities [4], etc., may lead to viable finite element forms in the years to come. However, as it stands, the use of three-dimensional elasticity in the finite element form appears to be the only feasible approach for obtaining stresses in the required detail, to ensure laminate integrity, until at least some of the recent theoretical models are converted into finite element forms and validated for application to laminate edge stress situations.

There are several studies in the literature employing three-dimensional finite elements for estimating stresses in the critical regions of the laminates [5–10]. Unfortunately, the use of three-dimensional elements not only increases demands on computer memory requirement but also increases the cost.

In view of the large computational effort involved, some ingenuity in the choice of the finite element grid helps in three-dimensional finite element analyses. A graded finite element mesh is often resorted to, with an adequate level of refinement in critical regions involving high stress gradients. More recently global–local analyses have been considered [11], wherein the local solution with appropriate displacement boundary conditions generated from the global solution yields the stress field in the local regions. This is essentially a two-stage analysis and much scope exists in terms of defining the local regions and the finite element grid in a successive manner to obtain all the necessary details. Usually both the local and the global solutions are obtained using the same elements which, of course, is not essential.

In this paper, we attempt an alternative possibility; namely, in the region where the three-dimensional elements are essential, the three-dimensional elements are employed with the rest of the region idealized in terms of appropriate simpler elements. A transition element connects both the regions smoothly to obtain the solution in the critical region to the desired accuracy in one stage. This approach has been utilized successfully in the past in studying boundary stresses in box-beams [12], shells [13] and swept plates [14]. In [15], some preliminary results of the free edge problem using this approach were presented. In the present study, free edge stresses in a $[0/90]_s$ laminated coupon are obtained by employing this approach. Quasi-three-dimensional eight-noded elements (Q3D8) are used in the region near the free edge and quasi-three-dimensional two-noded elements (Q3D2) in the rest of the region, interconnecting these two regions with transition elements. With this idealization it has been possible to obtain the edge stress field with much less computational effort, when compared to the complete three-dimensional idealization.

DESCRIPTION OF THE PROBLEM

The problem under consideration is that of analysis of a typical multi-layered, long, rectangular, laminated composite coupon subjected to remote uniform axial strain loading (see Fig. 1). The laminate is symmetric about the midplane and in each half it has an arbitrary number of plies, each with different thickness and fibre orientation. In such a laminate, a quasi-three-dimensional state of stress exists and the displacements u, v and w of any point on the cross-section represented by an $x = \text{constant}$ plane (Fig. 1b) are given by (see [16])

$$u(x, y, z) = \epsilon_0 x + U(y, z)$$
$$v(x, y, z) = V(y, z)$$
$$w(x, y, z) = W(y, z). \tag{1}$$

In such a case U, V and W are functions of y and z only. The axial strain, ϵ_0, is uniform along the x-axis. Consequently the gradients of U, V and W with respect to the x co-ordinate are zero. Hence the finite element model required to solve this basically three-dimensional problem is essentially two-dimensional.

The quasi-three-dimensional (Q3D) analysis reduces the problem size very significantly as compared to three-dimensional analysis. A number of investigators have studied this problem and valuable data are available. Hence this problem is chosen here to study the present concept of employing appropriate elements in different regions. For simplicity, a four-ply $[0/90]_s$ laminate, as shown in Fig. 2a, with the width $b = 20h$, has been considered as an illustrative example to demonstrate the economy attainable in the present approach. h is the thickness of each individual ply. Considering the double symmetry of the problem, one quarter of the cross-section as shown shaded in Fig. 2b is required to be considered for the analysis.

The same material properties of laminate as used in [17], repeated below, are used for the numerical studies.

$$E_{11} = 137.90 \text{ GPa} \quad (20.00 \times 10^6 \text{ psi})$$
$$E_{22} = E_{33} = 14.48 \text{ GPa} \quad (2.10 \times 10^6 \text{ psi})$$
$$G_{12} = G_{23} = G_{13} = 5.86 \text{ GPa} \quad (0.85 \times 10^6 \text{ psi})$$
$$\nu_{12} = \nu_{23} = \nu_{13} = 0.21.$$

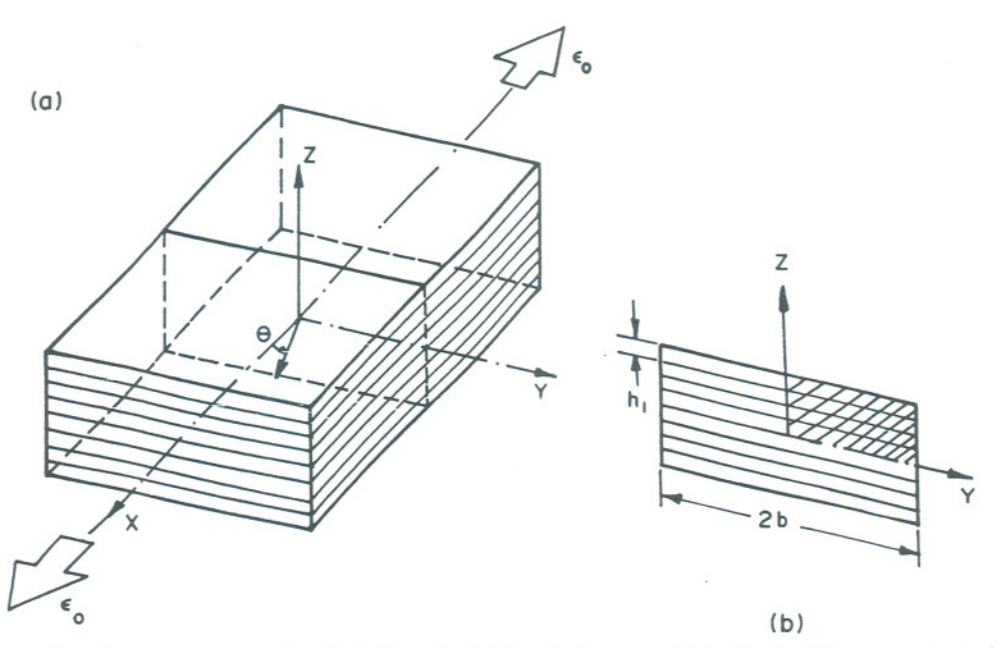

Fig. 1. Laminate geometry and analysis domain. (a) A typical symmetric laminate. (b) $x = \text{constant}$ plane.

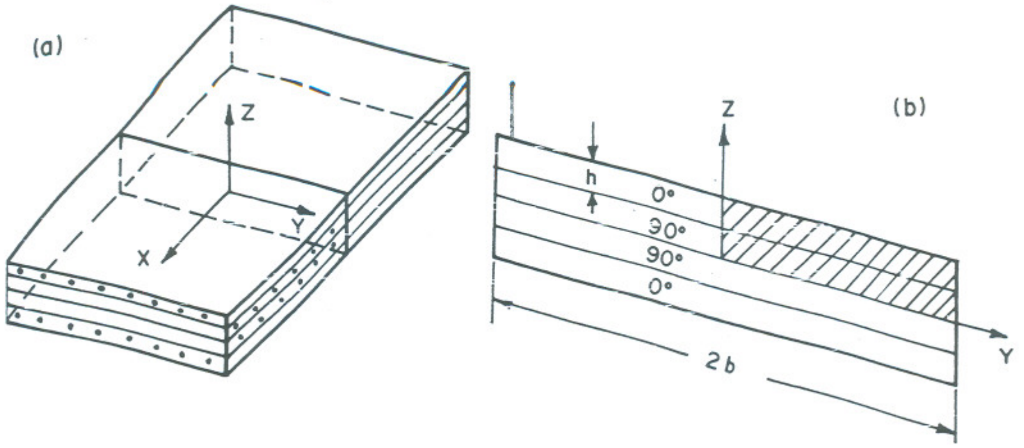

Fig. 2. (a) Four-ply $[0/90]_s$ long rectangular laminate. (b) Representative plane, x = constant.

Subscripts 1, 2 and 3 for the individual unidirectional ply correspond to the longitudinal, transverse and thickness directions, respectively, i.e. the material axes system.

CONVENTIONAL QUASI-THREE-DIMENSIONAL FINITE ELEMENT ANALYSIS

The quasi-three-dimensional finite element approach was developed in [17, 18] employing quasi-three-dimensional three-noded constant strain triangular elements to investigate the stress field in symmetrically laminated composites of finite dimensions. The mechanical (uni-axial tension), thermal and hygroscopic loads were considered. In [19], four- and eight-noded isoparametric quasi-three-dimensional quadrilaterals have been developed and several quasi-three-dimensional solutions have been reported [20–25] in the literature.

We first proceed to consider analysis of the $[0/90]_s$ laminate employing quasi-three-dimensional eight-noded parabolic quadrilateral isoparametric finite element (Q3D8). A typical finite element mesh adopted here is shown in Fig. 3, which represents the shaded region shown in Fig. 2b. A uniform extension case $\epsilon_0 = 1$ was considered.

The finite element idealization is graded in such a way that the smallest element size in the vicinity of the interface and near the free edge or the delamination tip, as the case may be, is $(h/4 \times h/4)$. An idealization with 65 elements and 232 nodes was employed to obtain numerical results. Distributions of displacements and stresses, including interlaminar stresses, were obtained. The symmetric edge delamination of depth $h/4$ located at either $z = 0$ or $z = \pm h$ was also considered to obtain stresses as well as the strain energy release rates. The results of the above analyses are used later as a benchmark solution for comparison with those obtained from the proposed scheme. A close examination of the results is provided below in order to indicate that the use of dissimilar elements in different regions is appropriate in order to gain certain computational advantages.

To begin with, the displacements v and w all over the cross-section of the laminate are examined in detail (see Figs 4–7). The value v along the y-axis is shown plotted in Fig. 4, for various z = constant planes. Figure 5 shows variation of v along the z-axis, for various values of y. It is clear that the variation of v along the z direction is negligibly small except near the free edge, i.e. within a distance of about 4–6h from the free edge. The variation of w shown in Figs 6

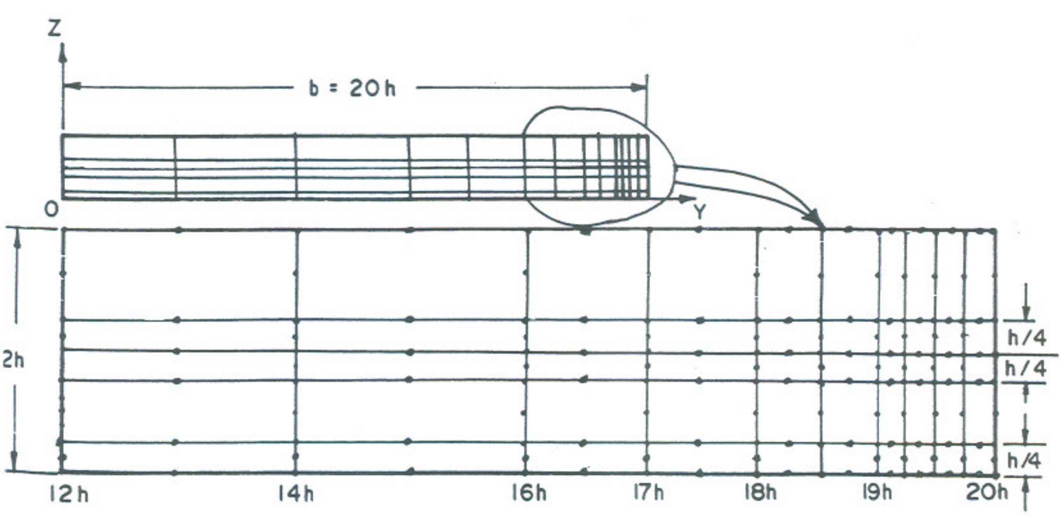

Fig. 3. Finite element model: Q3D8 analysis.

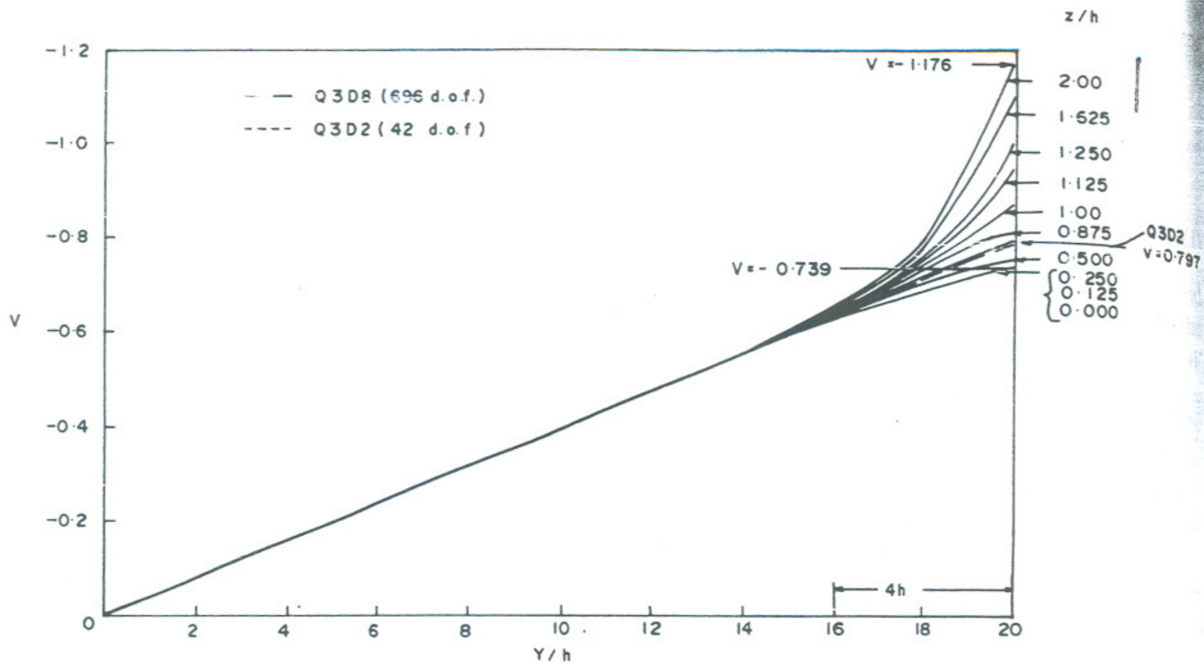

Fig. 4. Displacement v along the width of the laminate.

and 7 leads to a similar observation. w variation across the thickness at various $y = \text{constant}$ planes (shown in Fig. 7) suggests that the near-linear variation w across the thickness is established within a distance which is of the order of a ply thickness h from the free edge. It may be noted that at the free edge ($y = 20h$), w variation across the thickness is a bit unusual and seems to involve a normal strain ϵ_z discontinuity at the interface, which is of course admissible from elasticity considerations. It is clear that this phenomenon is associated with a very small region near the free edge. Stress variations along the y- and z-axis (not shown here) also indicate that the nature of stresses is three-dimensional only in a small region near the boundary. This provides the basis for the present approach, namely to use three-dimensional elements in a small region near the boundary and more simple elements elsewhere.

COMBINED USE OF Q3D2, TRANSITION AND Q3D8 FINITE ELEMENTS

It is now clear that rigorous three-dimensional idealization employing Q3D8 elements is essential only in a small portion near the free edge (region III, Fig. 8a) and in the rest of the cross-section (region I) a more simple treatment would be adequate. In [26], this concept has been utilized. A simple continuum

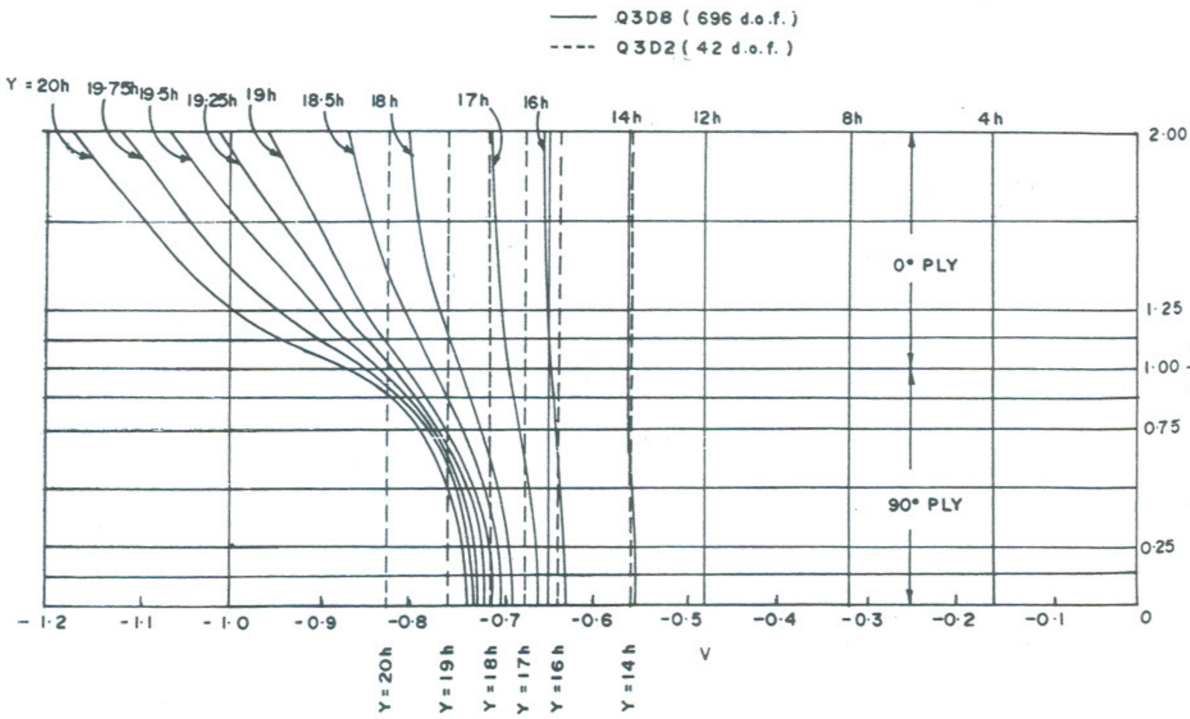

Fig. 5. Displacement v across the thickness of the laminate.

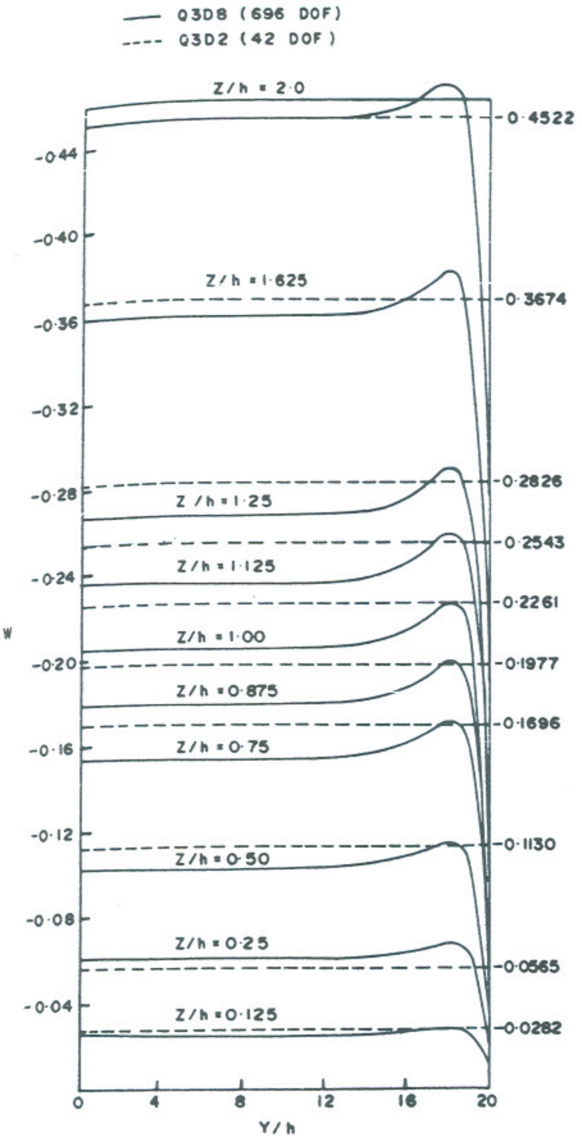

Fig. 6. Displacement w along the width of the laminate.

solution based on CLPT was obtained in region I and matched with the finite element solution in region III. In the present studies, region I is idealized in the finite element form so that it becomes somewhat general in terms of developing the computer program. Figure 8b shows a typical finite element idealization.

Region I: Q3D2 elements (Appendix)
Region II: Q3DT elements (description follows)
Region III: Q3D8 elements (eight-noded quasi-three-dimensional isoparametric quadrilateral elements [19]).

This idealization is denoted by $b1/h$–$b2/h$–$b3/h$, indicating the range of regions I, II and III, respectively. For example, 16–1–3 idealization indicates that region I covers the laminate width of $16h$ (Q3D2 elements), region II convers the distance of h (Q3DT: transition zone) and region III covers a width of $3h$ (Q3D8: quasi-three-dimensional eight-noded elements).

Q3DT: TRANSITION ELEMENT

In the present approach, different regions are modelled using elements with different nodal variables. In order to achieve smooth connectivity of the different regions an element with different types of nodes on its boundary becomes necessary. Such an element or zone is called here an 'interphase or transition element or zone'. Such elements were used earlier in [12–15].

Figure 9 describes the concept in the present case. The transition region is first formed as an assembly of n Q3D8 elements and then suitable constraints are

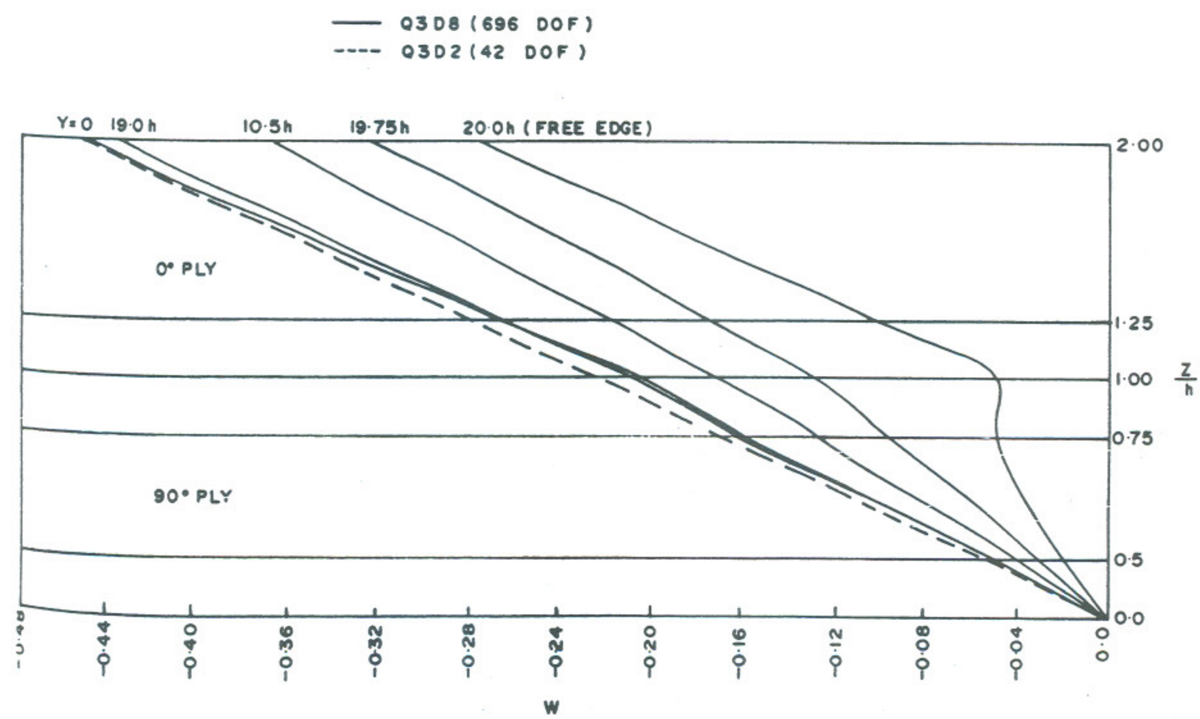

Fig. 7. Displacement w across the thickness of the laminate.

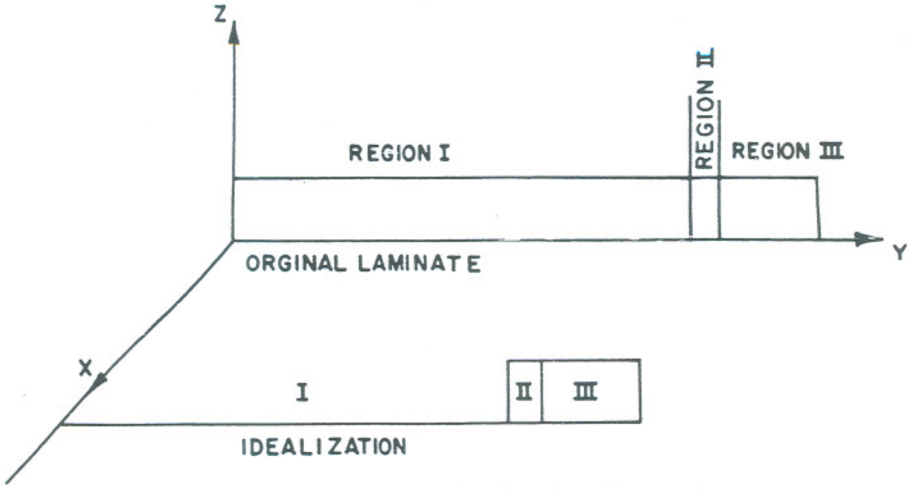

Fig. 8a. Idealization of the laminate into three regions.

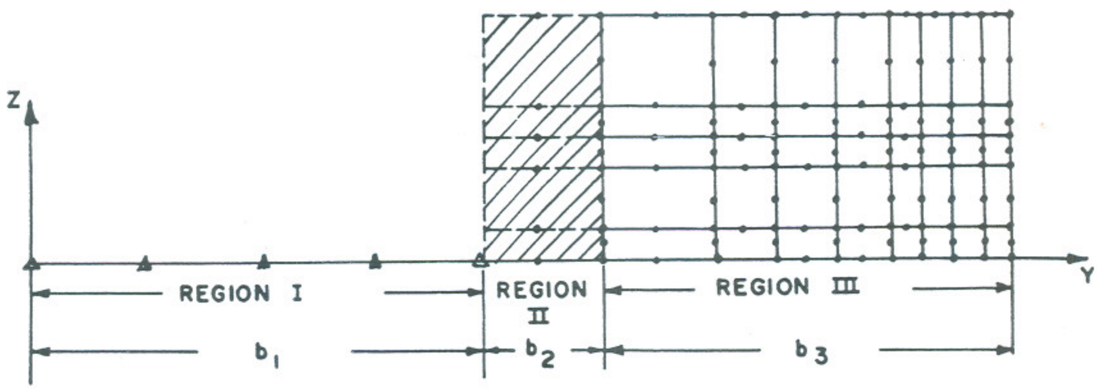

Fig. 8b. A typical finite element idealization of the three regions with (Q3D2–Q3DT–Q3D8) elements.

imposed on nodes located on the boundary with region I so that these nodes are converted, on transformation, into a single node, that can conveniently be attached to the node of the region I. The procedure involves the following steps.

The nodal displacement vector for the jth node of the untransformed or uncondensed transition element of Fig. 9a is given as

$$\delta_j^T = \{u \ \ v \ \ w\}j. \tag{2}$$

The vector of the global nodal displacements of the transition element before transformation would thus be

$$q^T = \{q_1^T \ q_2^T\}, \tag{3}$$

where

$$q_1^T = \{\delta 1 \ \ \delta 2 \ \ldots \ \delta j \ \ldots \ \delta m\}, \quad m = 3n + 2$$

and

$$q_2^T = \{\delta m + 1 \ \ \delta m + 2 \ \ldots \ \delta m + p\}, \quad p = 2n + 1,$$

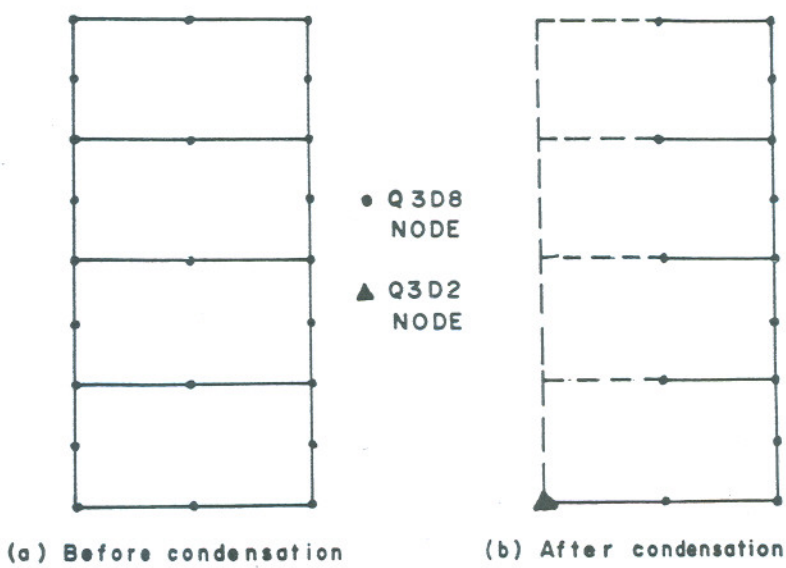

Fig. 9. Transition element before and after condensation.

where q_1 represents degrees of freedom remaining unaltered and q_2 represents degrees of freedom to be modified to achieve connection with region I.

Let $[K]$ be the assembled stiffness matrix of the interphase region and $\{r\}$ the load vector corresponding to the displacement vector $\{q\}$. The strain energy of this region can then be expressed as

$$U = 1/2\{q^T\}[K]\{q\}. \tag{4}$$

The vector of displacements that would represent the transition zone while assembling the global stiffness matrix, i.e. after suitable transformation, would be considered in the form

$$\{\bar{q}^T\} = \{\bar{q}_1^T \ \bar{q}_2^T\}, \tag{5}$$

where

$$\bar{q}_1 = q_1 \quad \text{and} \quad \bar{q}_2 = \bar{\delta}_{m+1},$$

where $\bar{\delta}_{m+1}$ is the vector of nodal degrees of freedom corresponding to the connecting Q3D2 node of region I given by

$$\{\bar{\delta}'^T_{m+1}\} = \{u \ v \ w\}_{m+1}.$$

The transformation between vector $\{q_2\}$ and $\{\bar{q}_2\}$ can be obtained through simple kinematically consistent relationships between three displacements assigned to each of the p nodes ($m+1$ to $m+p$) and three degrees of freedom offered by the Q3D2 node, i.e. the $(m+1)$th node.

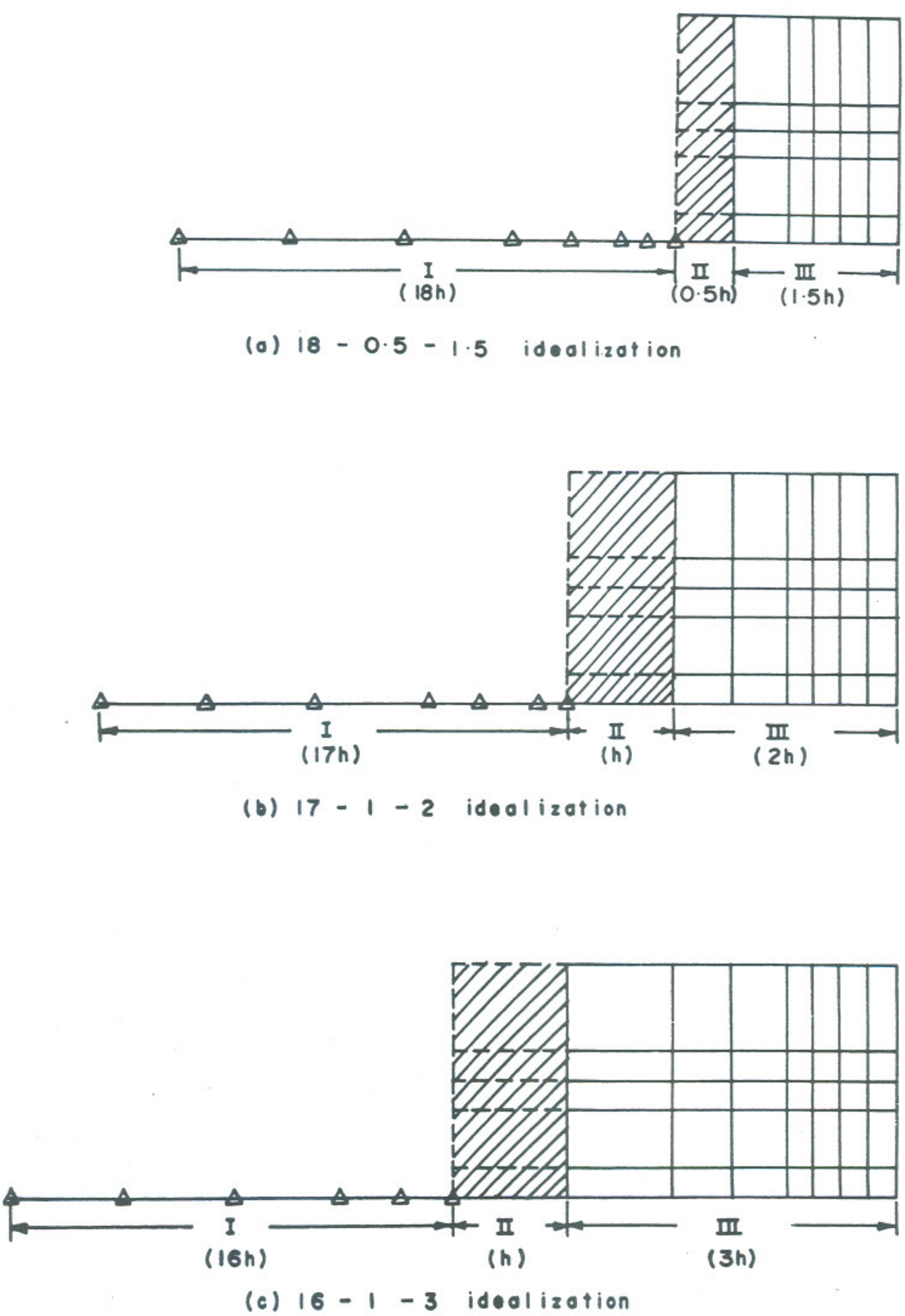

Fig. 10. Idealizations to study the effect of location of transition region.

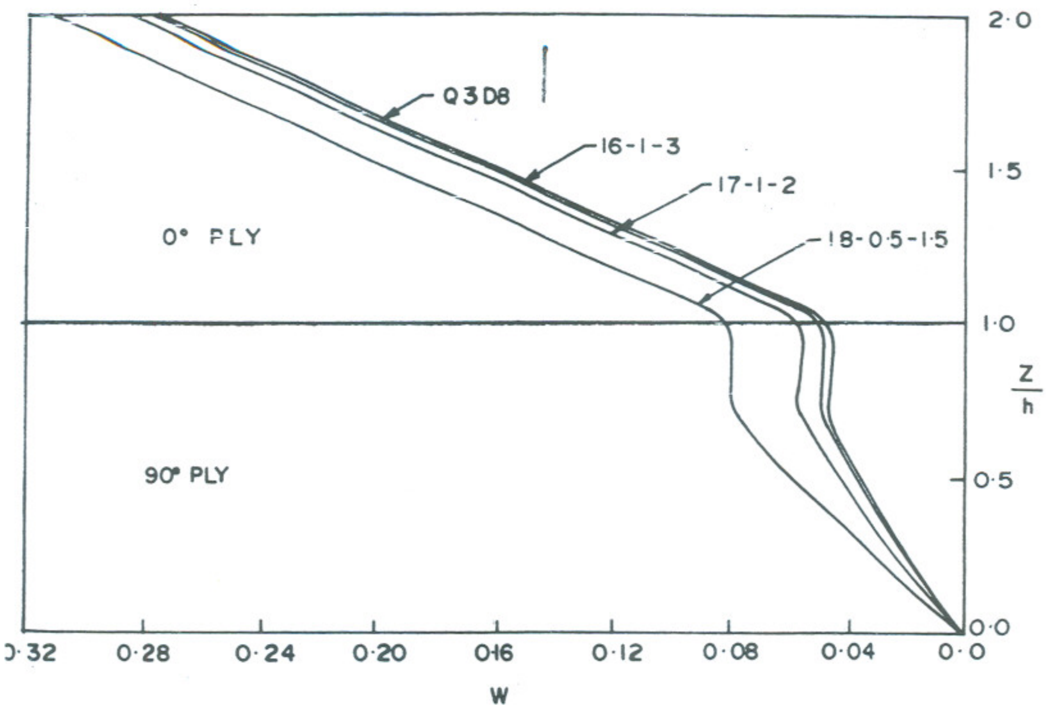

Fig. 11. w variation at $y = b$ (convergence study).

In matrix form this will appear as

$$\{q_2\} = [T_l]\{\bar{q}_2\} = \begin{bmatrix} T1 \\ T2 \\ \vdots \\ T_j \\ \vdots \\ Tp \end{bmatrix} \{\bar{q}_2\}, \tag{6}$$

where a typical submatrix Tj of the $(m + j)$th Q3D8 node would be

$$Tj = \begin{bmatrix} 1 & 0 & 0 \\ 0 & 1 & 0 \\ 0 & 0 & \zeta m + j \end{bmatrix}.$$

The strain energy of the transition (super) element (Fig. 9b) after condensation can now be written as

$$U = 1/2\{\bar{q}^T\}[T^T][K][T]\{\bar{q}\}, \tag{7}$$

where

$$[T] = \begin{bmatrix} I & 0 \\ 0 & T_l \end{bmatrix}$$

is of dimension $3(m + p) \times 3(m + 1)$, where I is the unit matrix of dimension 3 m. Thus

$$K_T = T^T K T \quad \text{and} \quad r_T^T = T^T r, \tag{8}$$

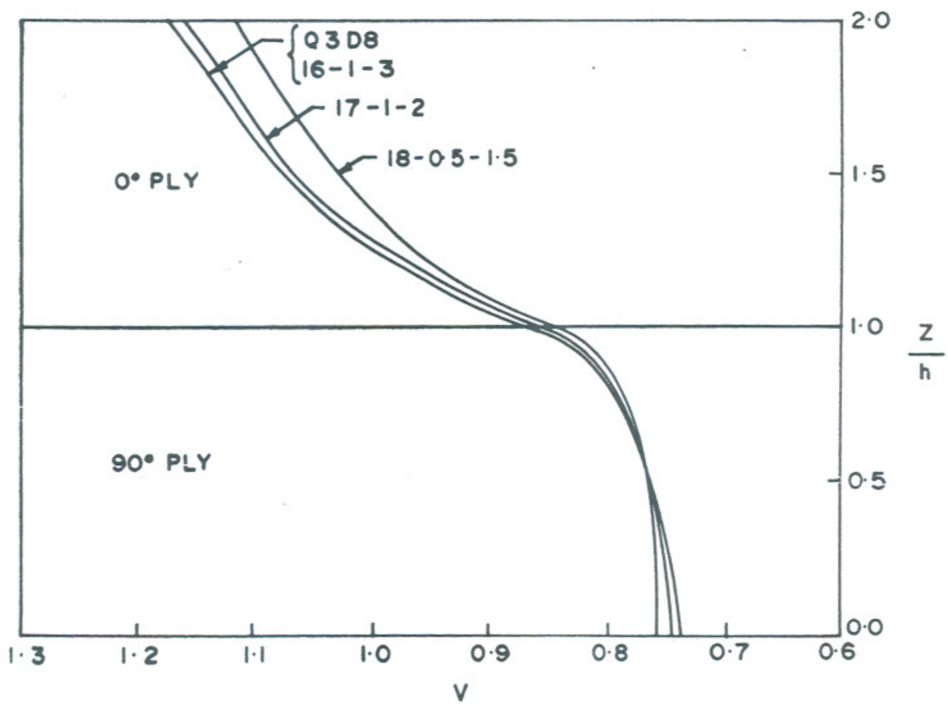

Fig. 12. v variation at $y = b$ (convergence study).

where K_T is the stiffness matrix and r_T is the load vector of the transition zone.

RESULTS AND DISCUSSIONS

Figures 10a, b and c show the finite element idealization used in the present study. Figures 11 and 12 show the values w and v across the thickness at a typical section $y = b$ for the three finite element idealizations. Clearly, as the three-dimensional region size increases, i.e. as the transition zone moves away from the free edge, the results approach the classical three-dimensional results. In the present case 16–1–3 idealization gives results very close to the benchmark values. Tables 1 through 4 display the convergence trend with reference to the stresses. These comparisons clearly indicate the adequacy of 16–1–3 idealization for bringing out the edge stress behaviour of the laminate.

Table 1. Stress σ_x variation ($y = b$) across the thickness

Z/h	18–0.5–1.5	17–1–2	16–1–3	Q3D8
0.500	14.8464	14.9281	14.9514	14.9591
1.625	137.8290	137.8310	137.8300	137.8300

Table 2. Stress σ_x variation along the width ($z = 1.125h$, 0° ply)

y/h	18–0.5–1.5	17–1–2	16–1–3	Q3D8
0.00	139.5400	139.5400	139.5300	138.4200
8.00	139.5400	139.5400	139.5400	138.4200
16.00	139.5400	139.5400	138.3900	138.3860
18.00	138.1400	138.2100	138.2340	138.2400
18.50	138.1020	138.1450	138.1590	138.1630
19.00	138.0470	138.0760	138.0850	138.0850
19.25	138.0250	138.0450	138.0490	138.0510
19.50	138.0030	138.0170	138.0190	138.0200
19.75	137.9560	137.9640	137.9660	137.9660
20.00	137.8290	137.8310	137.8300	137.8300

Table 3. Stress σ_y variation along the width ($z = 1.125\,h$, 0° ply)

y/h	18–0.5–1.5	17–1–2	16–1–3	Q3D8
18.000	1.8399	2.0291	2.0770	2.0993
18.500	1.8469	1.9486	1.9898	2.0032
19.000	1.7862	1.8513	1.8787	1.8836
19.250	1.7072	1.7559	1.7711	1.7784
19.500	1.5494	1.5810	1.5905	1.5940
19.750	1.1294	1.1438	1.1474	1.1482
19.875	0.6509	0.6532	0.6523	0.6518

Table 4. Stress σ_y variation along the width ($z = 0.875h$, 90° ply)

y/h	18–0.5–1.5	17–1–2	16–1–3	Q3D8
18.000	−4.1227	−3.8684	−3.6224	−3.4648
18.500	−3.9126	−3.6981	−3.5356	−3.4170
19.000	−3.4981	−3.3478	−3.2679	−3.1804
19.250	−3.1090	−3.0032	−2.9244	−2.8888
19.500	−2.5275	−2.4673	−2.4230	−2.4020
19.750	−1.5234	−1.5061	−1.4922	−1.4855
19.875	−0.4156	−0.4212	−0.4228	−0.4234

Figure 13 shows a comparision of interlaminar stresses in the spanwise direction and Fig. 14 shows the same in the thicknesswise direction. The results are in close agreement.

Figures 15a and b show the finite element idealization at the delamination tip, used to calculate the strain energy release rates. Following [27], the individual components of strain energy release rates in Mode I of fracture are computed as

$$G_{\rm I} = -\frac{1}{2\Delta}[Fz_B(W_D - W_{D'}) + Fz_A(W_C - W_{C'})],$$

where Fz_B is the force in the z-direction at node B, W_D is the displacement in z-direction at node D, etc. (see Fig. 15). Expressions used for $G_{\rm II}$ and $G_{\rm III}$ are obtained by replacing Fz with Fy and Fx and W with V and U, respectively.

Various components of forces and displacements at the required locations as estimated in the three idealizations considered are shown in Tables 5 and 6 for symmetric edge delaminations of depth $h/4$ at $z = 0$ and $z = \pm h$, respectively. The comparisons indicate that with the 16–1–3 idealization it is possible to estimate strain energy release rates reasonably accurately. Considering that the total number of

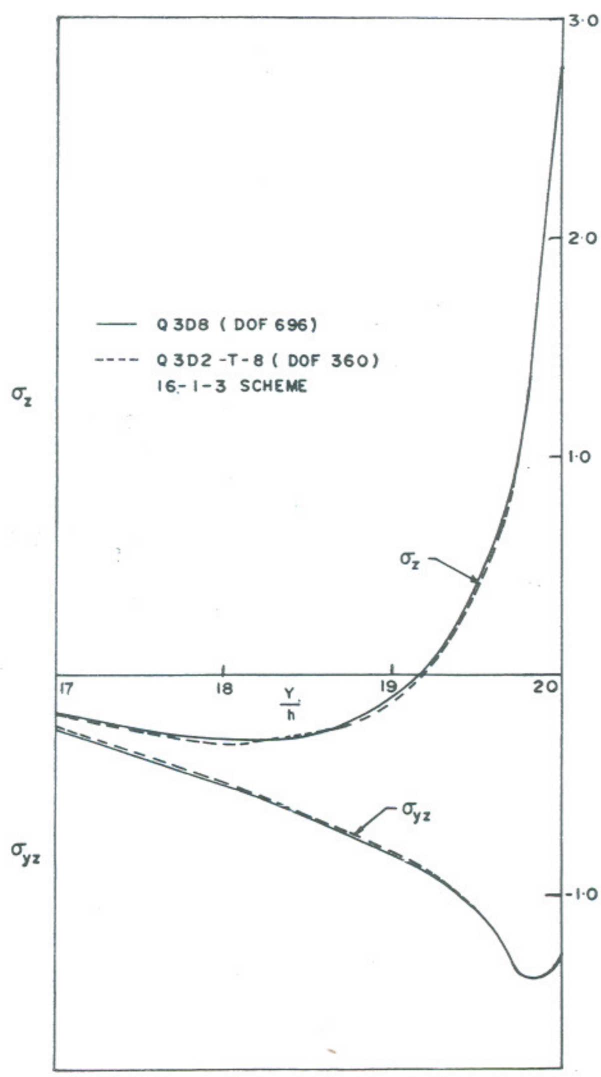

Fig. 13. σ_z and σ_{yz} variations along y-axis near free edge.

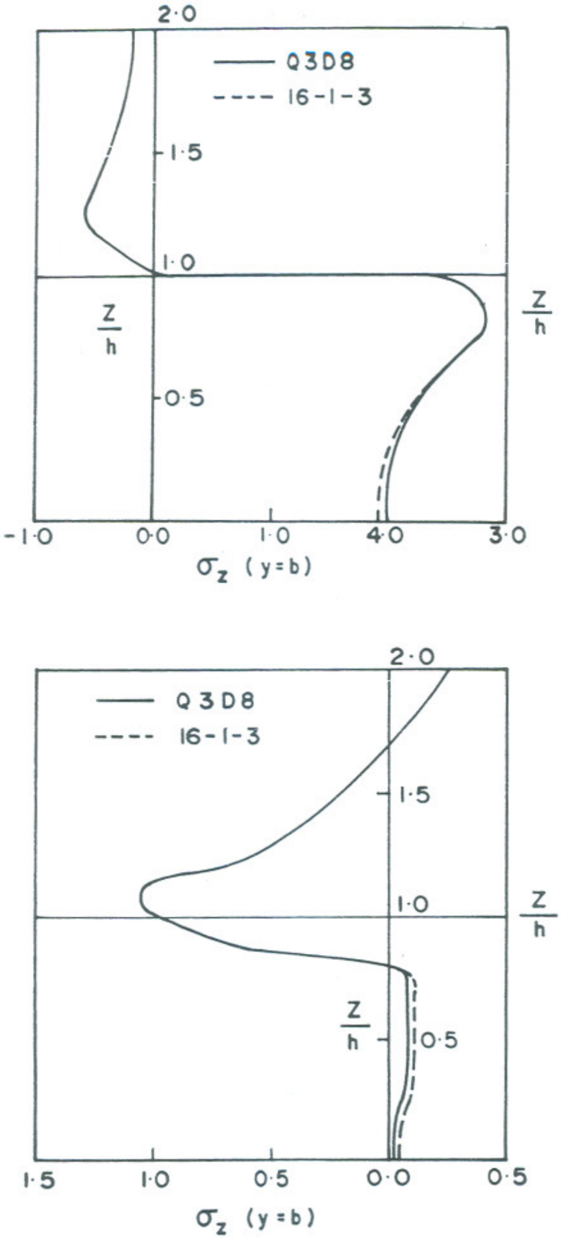

Fig. 14. σ_2 and σ_{yz} variations along z-axis at $y = b$.

degrees of freedom involved in 16–1–3 analysis is 360, which is much less than for the corresponding complete three-dimensional analysis, the present scheme may be considered expedient for the edge stress and edge delamination problem.

Table 5. Forces, displacements and strain energy rates. Edge delamination of depth $h/4$ at $z =$

Scheme/Pt	18–0.5–1.5	17–1–2	16–1–3	(Q
Forces Fz in the G calculation				
B	−0.2168	−0.3023	−0.3325	−(
A	−0.1588	−0.2248	−0.2476	−(
Displacements w in the G calculation				
D	0.0781	0.1103	0.1221	(
C	0.0541	0.0761	0.0840	(
Strain energy release rates (mode I: 100%)				
G_I	0.0510	0.1009	0.1228	(

Table 6a. Forces, displacements and strain energy rates. Edge delaminations of depth $h/4$ at $z =$

Scheme/Pt	18–0.5–1.5	17–1–2	16–1–3	Q
Forces Fy in the G calculation				
B	0.2969	0.3039	0.3056	
A	0.1551	0.1716	0.1755	
Displacements v in the G calculation				
D	−0.0703	−0.0711	−0.0713	−
C	−0.0380	−0.0386	−0.0387	−
Strain energy release rates (mode II)				
G_{II}	0.0535	0.0564	0.0571	
%	50.74	44.85	44.04	4

Table 6b. Forces, displacements and strain energy rates. Edge delaminations of depth $h/4$ at $z =$

Scheme/Pt	18–0.5–1.5	17–1–2	16–1–3	(
Forces Fz in the G calculation				
B	−0.2177	−0.2514	−0.2575	−
A	−0.1012	−0.1303	−0.1369	−
Displacements w in the G calculation				
D	0.0906	0.1017	0.1032	
C	0.0619	0.0699	0.0711	
Strain energy release rates (mode I)				
G_I	0.0520	0.0694	0.0726	
%	49.26	55.15	55.96	5

CONCLUSIONS

Problems involving three-dimensional anal quire a large number of degrees of freedom a attempt to reduce the size of the problem with of accuracy will be of great help. In this pa attempt is made to achieve this objective by e ing appropriate elements in the different reg

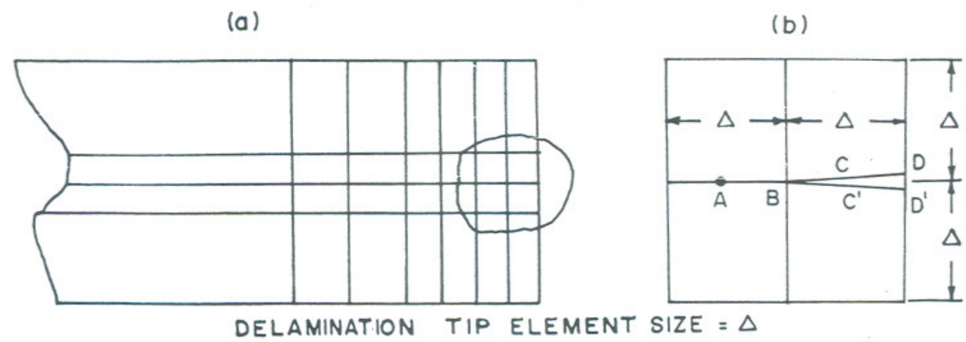

Fig. 15. Nodes used in the strain energy release rate computations. (a) Finite element mesh at free edge. (b) Delamination.

the structure. Edge stress analysis of laminated test coupons with and without delamination has been considered to illustrate the concept. Displacements, stress distributions and strain energy release rates are estimated using the present approach and compared with those obtained from the full quasi-three-dimensional analysis. Results indicate that this approach is highly promising.

Acknowledgement—The authors are grateful to Dr I. S. Raju for the useful discussions they had with him and for the computer code which he made available to the authors.

REFERENCES

1. N. J. Pagano, Stress field in composite laminates. *Int. J. Solids Struct.* **14**, 385–400 (1978).
2. N. J. Pagano and S. R. Soni, Global–local laminate variational model. *Int. J. Solids Struct.* **19**, 207–218 (1983).
3. A. V. Krishna Murty, Theoretical modelling of laminated composite plates. *Proc. Indian Acad. Sci. Sadhana* **II**, 357–365 (1987).
4. K. Vijayakumar and A. V. Krishna Murty, Iterative modelling for stress analysis of composite laminates. *Int. J. Comp. Sci. Technol.* **32**, 165–181 (1988).
5. D. J. Wilkins, R. A. Eisenmann, R. A. Camin, W. S. Morgolis and R. A. Benson, Characterising delamination growth in graphite epoxy. *Damage in Composite Materials*, ASTM STP 775 (1982).
6. L. Carlsson, Interlaminar stresses at a hole in a composite member subjected to in-plane loading. *J. Comp. Mater.* **17**, 238–249 (1983).
7. A. S. D. Wang, N. N. Kishore and C. A. Li, A three-dimensional finite element analysis of delamination growth in composite laminates, part 2. The finite element code and users' manual, NADC-TR-84018-60 (1983).
8. K. Ericson, M. Persson, L. Carlsson and A. Gustavsson, On the prediction of the initiation of delamination in a $[0/90]_s$ laminate with a circular hole. *J. Comp. Mater.* **18**, 495–506 (1984).
9. M. N. Janardhana, K. C. Brown and R. Jones, Designing for tolerance to impact damage at fastner holes in graphite/epoxy laminates under compression. *J. theor. appl. Fract. Mech.* **5**, 51–55 (1986).
10. P. L. N. Murthy and C. C. Charmis, Composite interlaminar fracture toughness: three-dimensional modelling for mixed mode I, II and fracture. In *Composition Materials: Testing and Design* (Eighth Conference) (Edited by J. D. Whitcomb), pp. 23–40. ASTM STP 972 (1988).
11. O. Hayden Griffin Jr and M. A. Vidussoni, Global/local finite element analysis of composite materials. In *CAD in Composite Material Technology* (Edited by C. A. Brebbia) (1988).
12. S. Sreedharmurthy and A. V. Krishna Murty Vibrations of aircraft wing-type structures. Report No. ARDB-STR 5004, Department of Aerospace Engineering, Indian Institute of Science (1976).
13. A. V. Krishna Murty and K. N. Shivkumar, Combined use of solid of revolution, thin-shell and interphase elements for the analysis of cylindrical shells. *J. struct. Mech.* **8**, 42–59 (1980).
14. B. R. Somashekar, A. V. Krishna Murty and C. S. Nanjunda Ram, A study of swept cantilever wings employing interphase element concept for structural reduction. *J. aeronaut. Soc. India* **35**, 77–105 (1983).
15. A. V. Krishna Murty and C. G. Shah, Finite element analysis of delaminated composite panels. Proc. ICES-88, Vol I, Atlanta, GA, 10–14 April 1988.
16. R. B. Pipes and N. J. Pagano, Interlaminar stresses in composite laminates under uniform axial extension. *J. Comp. Mater.* **4**, 538–548 (1970).
17. A. S. D. Wang and F. W. Crossman, Some new results of edge effects in symmetric composite laminates. *J. Comp. Mater.* **11**, 92–106 (1977).
18. A. S. D. Wang and F. W. Crossman, Edge effect in thermally induced stresses in composite laminates. *J. Comp. Mater.* **11**, 300–312 (1977).
19. I. S. Raju and J. H. Crew Jr, Interlaminar stress singularities at a straight free edge in composite laminates. *Comput. Struct.* **14**, 21–28 (1981).
20. J. D. Whitcomb, I. S. Raju and J. G. Goree, Reliability of the finite element method for calculating free edge stresses in composite laminates. *Comput. Struct.* **15**, 23–37 (1982).
21. J. D. Whitcomb and I. S. Raju, Superposition method for analysis of free edge stresses. *J. Comp. Mater.* **17**, 492–507 (1983).
22. T. K. O'Brien, Characterisation of delamination onset and growth in a composite laminate. *Damage in Composite Materials*, ASTM STP 775, pp. 140–167 (1982).
23. K. S. Kim and C. S. Hong, Delamination growth in angle-ply laminated composites. *J. Comp. Mater.* **20**, 423–438 (1986).
24. T. K. O'Brien, I. S. Raju and D. P. Garber, Residual thermal and moisture influences on the strain energy release rate analysis of edge delamination. *J. Comp. Technol. Res.* **8**(2), 37–47 (1986).
25. I. S. Raju, J. H. Crews Jr and M. A. Aminpour, Strain energy release rate components for edge-delaminated composite laminates. *Engng Fract. Mech.* 383–396 (1988).
26. W. S. Chan, C. Rogers and S. Aker, Improvement of edge delamination strength of composite laminates using adhesive layers. *Composite Materials: Testing and Design*, ASTM STP 893, pp. 266–285 (1986).
27. I. S. Raju, Q3DG—a computer program for strain energy release rates for delamination growth in composite laminates, NASA CR-178205 (1986).

APPENDIX: ELEMENT Q3D2

A simple element, appropriate for idealization of region I of the laminate under consideration (Fig. 8a) is given here. The geometry and the coordinate system of a typical element are shown in Fig. A1.

Displacement field

$$\Delta = \Delta_0 + A_\delta \delta, \tag{A1}$$

where

$$\{\delta\} = \{U \;\; V \;\; W\},$$

$$\Delta_0 = \begin{Bmatrix} \epsilon_0 x \\ 0 \\ 0 \end{Bmatrix} \quad A_\delta = \begin{bmatrix} 1 & & \\ & 1 & \\ & & \zeta \end{bmatrix}.$$

Shape functions

$$\{\delta\} = Aq\{q\}, \tag{A2}$$

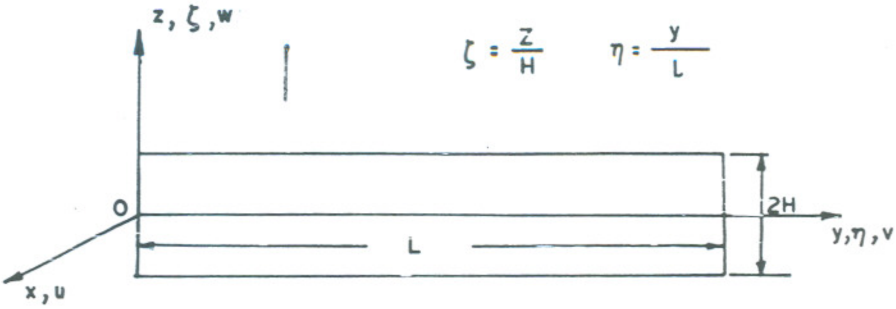

Fig. A1. Co-ordinate system and geometry for Q3D2 element.

where

$$Aq = \begin{bmatrix} F_1 & 0 & 0 & F_2 & 0 & 0 \\ 0 & F_1 & 0 & 0 & F_2 & 0 \\ 0 & 0 & F_1 & 0 & 0 & F_2 \end{bmatrix} \quad \text{(A3)}$$

$$\{q\}^T = \{u_1 \quad v_1 \quad w_1 \quad u_2 \quad v_2 \quad w_2\}$$

$$F_1 = 1 - \eta \quad F_2 = \eta.$$

The strain–displacement relations are

$$\epsilon = \Gamma\Delta,$$

where

$$[\Gamma] = \begin{bmatrix} \partial/\partial x & 0 & 0 \\ 0 & 1/1 \cdot \partial/\partial\eta & 0 \\ 0 & 0 & 1/H \cdot \partial/\partial\zeta \\ 0 & 1/H \cdot \partial/\partial\zeta & 1/1 \cdot \partial/\partial\eta \\ 1/H \cdot \partial/\partial\zeta & 0 & \partial/\partial x \\ 1/1 \cdot \partial/\partial\eta & \partial/\partial x & 0 \end{bmatrix}.$$

Strain field

$$\{\epsilon\}^k = \{\epsilon^*\} + [Bq]\{q\}, \quad \text{(A4)}$$

where

$$\epsilon^* = \{\epsilon_0 \quad 0 \quad 0 \quad 0 \quad 0 \quad 0\}$$

$$Bq = \Gamma A_\delta Aq.$$

Stress field

$$\{\sigma\}^k = [D]^k\{\epsilon\}^k. \quad \text{(A5)}$$

$[D]^k$ is the three-dimensional elasticity matrix of the kth layer.

Considering the expression for the strain energy U in the form

$$U = 1/2 \int_V \epsilon^T\sigma \, dV \quad \text{(A6)}$$

and using eqns (A1)–(A6), one obtains the stiffness matrix as

$$K = \sum_{k=1}^{N} \int_{\zeta_{k-1}}^{\zeta_k} \int_0^1 Bq^T(\eta,\zeta) D^k Bq(\eta,\zeta) \, d\eta \, d\zeta,$$

where N = number of plies in the laminate and a consistent load vector due to uniform axial strain as

$$r^T = \sum_{k=1}^{N} \int_{\zeta_{k-1}}^{\zeta_k} \int_0^1 \epsilon^{*T} D^k Bq(\eta,\zeta) \, d\eta \, d\zeta.$$

A two-point Gauss quadrature integration is adequate for numerical computation to obtain the elements of the stiffness matrix and the load vector.

Figures 4 through 7 show some results obtained using only this element to idealize the complete region of the cross-section. A total of 13 elements graded appropriately (see Fig. A2) is employed, involving only 42 equations as against 696 in the three-dimensional solution. Close agreement with the three-dimensional solution for displacements except near the free edge may be noted. Clearly this element is adequate to model 75–80% of the laminate in the region away from the free edge.

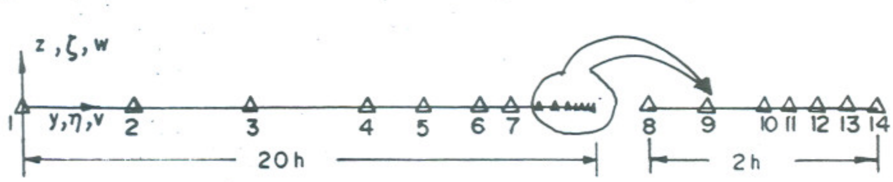

Fig. A2. Finite element idealization of the laminate using Q3D2.